



Radiative Influence of Dust Aerosols on the Evolution of Tropical Storm Hermine

Alexander Garber¹, Zhaoxia Pu¹, Anna Gannet Hallar¹

¹Department of Atmospheric Sciences, University of Utah, Salt Lake City, UT 84112, USA

5

Correspondence to: Alexander Garber (Alexander.Garber@utah.edu)

Abstract. This study investigates the impact of dust aerosols on the evolution of Tropical Storm Hermine (2022) using the Weather Research and Forecasting model coupled with Chemistry (WRF-Chem) and observational data from the NASA Convective Processes Experiment - Cabo Verde (CPEX-CV). The objective is to evaluate how varying initial dust aerosol

10 conditions influence storm development and to uncover the mechanisms behind these effects. Three WRF-Chem simulations were conducted with different initial aerosol concentrations: one with no aerosols, one with realistic dust concentrations, and one with intermediate aerosol levels. The simulations were compared against observational data from CPEX-CV and the best track data from the United States' National Hurricane Centre, focusing on parameters such as wind, pressure, aerosol optical depth, and radar reflectivity. The results indicate that the radiative effect of dust aerosols led to a weaker and more 15 disorganized storm system compared to simulations without the inclusion of dust, highlighting the critical role of dust-radiation interactions in modifying storm intensity. Furthermore, the study found that the ECMWF's Atmospheric Composition Reanalysis 4 (CAMS) underestimated atmospheric dust concentrations, in comparisons to observations, underlining the necessity for accurate observational data to validate aerosol-related processes and improve model predictions. These findings emphasize the complexity of dust aerosol-storm interactions and the importance of improving 20 aerosol representations in simulations of tropical cyclones.

1 Introduction

Tropical cyclones (TCs) are among the most destructive weather systems on Earth, and improving the accuracy of their forecasts remains a central goal in tropical meteorology. Modern numerical weather prediction models have significantly advanced forecast skill, but their accuracy depends critically on the representation of physical processes (DeMaria et al., 25 2007). In particular, the evolution of TCs is strongly influenced by their surrounding thermodynamic and aerosol environment (Emanuel 2007; Takahashi et al. 2017; Bhatia et al., 2022). One key environmental feature in the North Atlantic is the Saharan Air Layer (SAL), a hot, dry, and dusty air mass originating from the Sahara Desert and advected westward over the Atlantic Ocean by the African easterly jet (Braun, 2010).

Saharan dust is frequently lofted into the mid-troposphere during boreal summer, with outbreaks typically occurring every



30 3–5 days. These plumes can extend thousands of kilometers from Africa, often interacting with African easterly waves (AEWs), the precursors of many Atlantic tropical cyclones. The dust is composed of particles with a broad but skewed size distribution, generally dominated in number by submicron particles but with larger particles contributing most of the total mass (Sajani et al., 2012; Chicea and Olaru, 2023). Particle size, composition, and vertical distribution all influence the optical and properties of the dust, and consequently its radiative and thermodynamic effects.

35 The role of Saharan dust in TC genesis and intensification remains a subject of active debate. Several modeling studies have shown that dust can suppress storm development through multiple mechanisms, including enhanced atmospheric stability, midlevel warming, and increased wind shear (e.g., Reale et al., 2009; Bercos-Hickey et al., 2017; Khain et al., 2009). Khain et al. (2009) found that elevated aerosol concentrations invigorated convection in the outer rainbands of Hurricane Katrina at the expense of the inner core, resulting in a weaker storm. Similarly, Zhang et al. (2007) demonstrated in idealized 40 simulations that polluted environments increased peripheral convection and rainfall but reduced storm organization and peak wind speeds. Dust can also modify cloud microphysics by acting as ice nuclei (IN), altering ice size distributions and phase partitioning (DeMott et al., 2003; Harrison et al., 2022). Radiative effects are also significant: absorbing dust layers reduce surface insulation while warming the mid-troposphere, potentially strengthening the SAL inversion and stabilizing the lower atmosphere (Bercos-Hickey et al., 2017).

45 However, other studies argue that the SAL's role in suppressing TC activity may be overstated. Braun (2010) suggested that SAL-related shear often remains peripheral to developing systems, while the enhanced African easterly jet can, under some conditions, focus convection towards the storm core and aid organization. Pan et al. (2018) further demonstrated that the net impact of dust depends on latitude, with more favorable conditions for TC formation north of 15°N but reduced activity to the south, reflecting shifts in the intertropical convergence zone and African easterly jet.

50 Despite decades of study, the net effect of Saharan dust on TC development is not fully resolved, partly due to a lack of coordinated modeling and observational analyses. Field campaigns offer critical opportunities to bridge this gap. In September 2022, NASA conducted the Convective Processes Experiment–Cabo Verde (CPEX-CV; Nowotnick et al., 2024) during the climatological peak of the Atlantic hurricane season. Based out of Sal Island, Cabo Verde, the campaign targeted AEWs and associated SAL outbreaks using the HALO research aircraft, equipped with in situ and remote sensing 55 instrumentation. Research Flights 09 and 10 sampled the disturbance that later became Tropical Storm Hermine, capturing detailed vertical profiles of temperature, humidity, winds, and aerosols. These observations revealed aerosol optical depths exceeding 3 near the storm, significantly higher than values in the Copernicus Atmosphere Monitoring Service (CAMS) reanalysis, which underestimated dust loading by roughly 50% in this case, based off aircraft data (see Section 3.1).

The availability of high-quality, coincident observational and reanalysis data for Hermine offers a rare opportunity to 60 investigate dust–storm interactions in a real-world setting while also testing the reliability of current aerosol reanalyses. In this study, the Weather Research and Forecasting model with chemistry (WRF-Chem) is used to simulate Hermine under three distinct dust-loading scenarios: a Clean case with no dust, an Intermediate case using unmodified CAMS dust fields, and an Extra case in which dust loading is enhanced to match the magnitudes of CPEX-CV observations. Comparing these



simulations allows us to quantify the influence of dust on storm intensity, structure, and thermodynamic environment, to
65 assess how well CAMS reanalysis represents observed dust conditions, and to evaluate the role that targeted field
observations can play in improving aerosol initialization in numerical weather prediction models.

2 Simulation description

70 Tropical Storm Hermine (2022) was a short-lived, late-September system that developed in the eastern tropical Atlantic from
a well-defined African easterly wave. The disturbance formed southwest of the Cabo Verde Islands in an environment
characterized by strong SAL influence, abundant mid-level moisture, and moderate vertical wind shear. Hermine reached
tropical storm strength on 23 September 2022, with maximum sustained winds of approximately 40 kt and a minimum
75 central pressure near 1000 hPa. The system's track was primarily toward the north-northwest, remaining over open waters
and never posing a direct threat to land. Despite its modest intensity, Hermine was notable for occurring during a period of
active SAL outbreaks, making it a useful case study for investigating dust–tropical cyclone interactions in the eastern
Atlantic basin (Reinhart 2023).

In this study, the meteorological environment of Tropical Storm Hermine and the associated dust fields were simulated using
version 4 of the Weather Research and Forecasting model coupled with Chemistry (WRF-Chem; Grell et al., 2005; Fast et al.,
80 2006). WRF-Chem is a fully online model in which meteorology, chemistry, and aerosol processes are integrated within a
single framework, allowing direct two-way interactions between atmospheric dynamics and composition. This coupling
enables the representation of feedbacks between aerosols, radiation, clouds, and precipitation, which is critical for studying
dust–storm interactions in a physically consistent manner. The model was configured to explicitly represent both the
synoptic-scale flow and mesoscale features of the eastern tropical Atlantic during the study period.

85 Meteorological initial and lateral boundary conditions were provided by the European Centre for Medium-Range Weather
Forecasts (ECMWF) Reanalysis v5 (ERA5; Hersbach et al., 2020), chosen for its high spatial and temporal resolution and
demonstrated skill in capturing large-scale circulation patterns relevant to AEW and SAL environments. Chemical initial and
90 boundary conditions were obtained from the ECMWF Atmospheric Composition Reanalysis 4 (CAMS; Inness et al., 2019),
which offers global coverage at $0.75^\circ \times 0.75^\circ$ resolution. Although CAMS also provides meteorological variables, these
were not used in this study because their comparatively coarse resolution is insufficient to resolve the mesoscale structure of
tropical cyclones.

95 WRF-Chem includes multiple aerosol modules, each with distinct trade-offs in process complexity, computational demand,
and coupling options. For this study, the Model for Simulating Aerosol Interactions and Chemistry (MOSAIC; Zaveri et al.,
2008) was selected due to its detailed representation of aerosol and chemistry, its ability to couple directly with radiative
transfer and cloud microphysics schemes, and its active development status (Kazil, 2025). MOSAIC predicts aerosol mass
and composition, includes aqueous-phase chemistry, and supports both four-bin and eight-bin particle size distributions. The
four-bin configuration, used here, represents ultrafine, fine, coarse, and very coarse aerosol modes and is fully compatible



with the MOZBC (Model for Ozone and Related Chemical Tracers Boundary Conditions) preprocessing tool employed to map CAMS aerosol output to WRF-Chem size bins.

100 Because CAMS aggregates the largest dust sizes into a single coarse category spanning multiple WRF-Chem bins, the very coarse (.9- 20 um) bins in most simulations were initialized to zero. Given the rapid gravitational settling and deposition of large Saharan dust particles during trans-Atlantic transport, their omission was not expected to substantially bias particle number or mass concentrations in Hermine's environment (Knippertz and Todd 2021). In the no-dust (Clean) simulation, all dust-related coefficients were set to zero in the initial conditions to ensure dust-free initialization, although the model's dust
105 emission module did produce small amounts dynamically over land. These remained negligible compared to dust-present runs. In the enhanced-dust (Extra) simulation, initial dust coefficients were doubled to account for the ~50% underestimation of dust concentrations in CAMS relative to in situ observations from the CPEX-CV campaign. This setup provided a targeted sensitivity test to evaluate storm response under realistically observed versus underestimated dust loading conditions. Three primary simulations were used for the analysis: Intermediate, Clean, and Extra. Specifically, for Intermediate, the
110 simulation was conducted with a two-domain setup (Figure 1): an outer domain at 15 km resolution and an inner domain centered on Hermine at 3 km resolution. The outer domain, not cloud-permitting, used the Grell-3 cumulus parameterization scheme, which incorporates shallow convection and radiation interaction but excludes momentum tendencies (Grell, 1993). The inner domain, with resolution sufficient to explicitly resolve cumulus clouds, did not use cumulus parameterization. Cumulus radiation feedback was enabled for the outer domain but disabled for the inner domain.

115

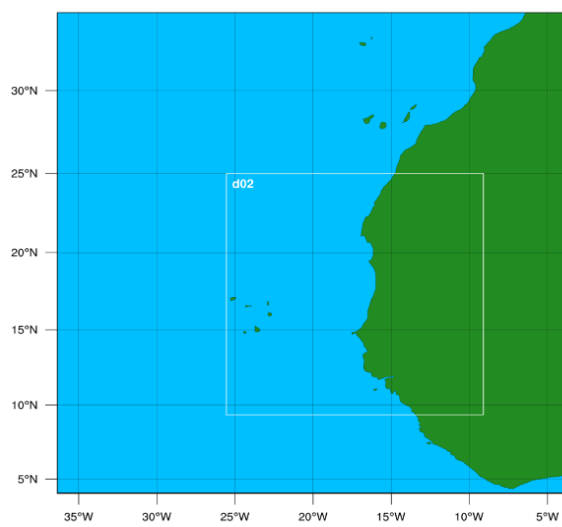


Figure 1. The model domain, with d02 indicating the inner domain.

Both domains employed the Purdue–Lin bulk microphysics scheme, which is widely used in high-resolution, real-data simulations (Chen and Sun, 2002). A limitation of this scheme is its bulk treatment of aerosols, which precludes explicit



120 representation of aerosol–cloud microphysical interactions. This limitation is appropriate for the present study, as the primary objective is to examine the radiative effects of dust rather than its indirect effects through cloud microphysics. Longwave radiation was represented using the Rapid Radiative Transfer Model, which uses lookup tables for computational efficiency (Mlawer et al., 1997). Shortwave radiation was handled using the CAM scheme, originating from the CAM 3 climate model, which allows for trace gas and aerosol interactions—important for this dust-focused study (Collins et al., 125 2004). Radiation calculations were performed every 5 minutes in both domains. The MOSAIC aerosol scheme was configured with aerosol dry deposition enabled and a hybrid dust option combining GOCART emissions with MOSAIC aerosols. Chemistry processes were updated every 90 seconds in the outer domain and every 30 seconds in the inner domain. The simulation covered the period from 00 UTC 21 September 2022 to 00 UTC 24 September 2022.

Clean used the same domains, physics, and chemistry configurations as Intermediate but with initial dust conditions set to 130 zero. While minimal dust was generated post initialization, the amount was negligible compared to dust-present runs. Extra was identical to Intermediate except that initial dust concentrations were doubled to better match observations from the CPEX-CV campaign, which indicated that CAMS underestimates dust levels. Across all simulations, initial humidity fields were identical, ensuring that dry Saharan air was present even in the no-dust run. This design allowed for isolation of dust aerosol effects from the known influence of dry air on tropical cyclone development. Additionally, no other aerosol types 135 were included in any run, ensuring that observed differences among simulations could be attributed solely to dust aerosol impacts.

3 Results and Analysis

3.1 Dust concentrations

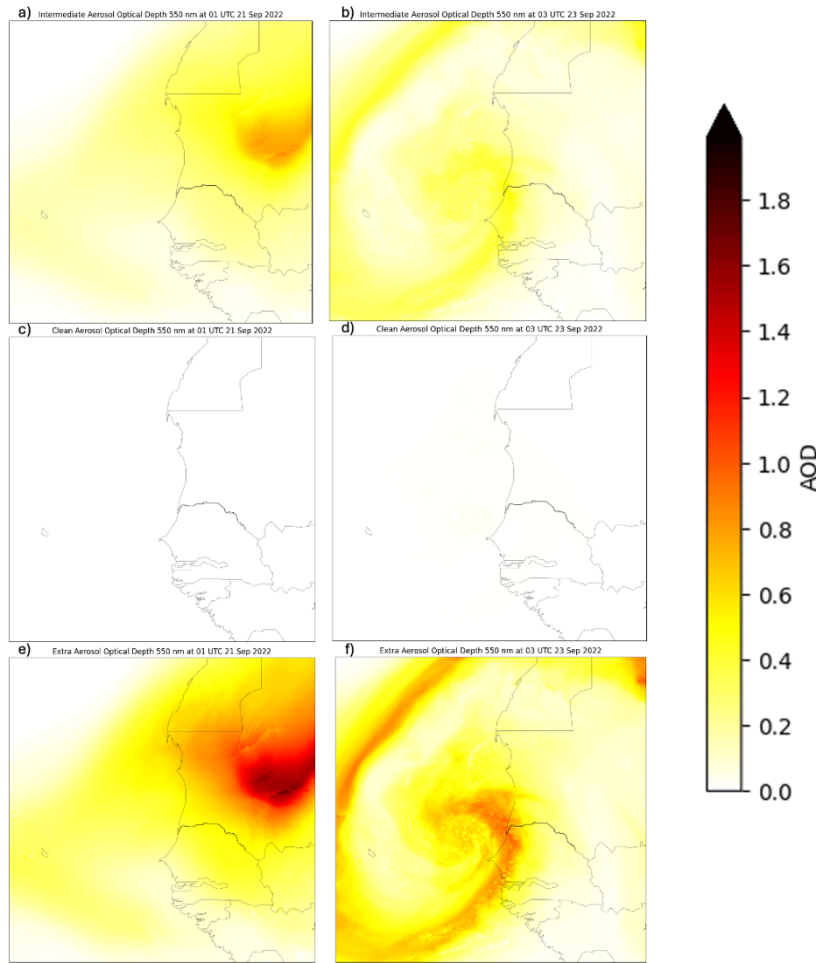
140 The first step in evaluating the simulations was to verify that the simulated dust loadings were realistic and comparable to observations. Since all model runs used CAMS data for initial and boundary conditions, the spatial positioning of dust at initialization matched the CAMS output. However, when compared CAMS with CPEX-CV observations, CAMS represented the initial dust plume location reasonably well but underestimated its magnitude. Peak aerosol optical depth (AOD) in CAMS was approximately 1.0, whereas CPEX-CV observations near Hermine reported values closer to 3.0 145 (Nowottnick et al., 2024).

To address this discrepancy, the mapping coefficients in the MOZBC program were doubled in the Extra simulation. This adjustment increased the dust loading to better approximate observed values. Runs without this adjustment (Intermediate) contained more dust than the no-dust control (Clean) but still less than observed during CPEX-CV.

AOD at 550 nm was used to quantify dust loadings at the start and end of the runs. In both Intermediate and Extra, the initial 150 plume placement matched CAMS, and dust was advected into Hermine's circulation (Figure 2). Clean started with no dust; although some Saharan dust was generated during the run, its contribution was negligible. Extra displayed the highest initial



AOD, approaching 2.0—lower than peak RF 09 observations but likely muted by model resolution. By the end of each simulation, dust was partially scavenged but remained significant in the dust-present runs.



155 **Figure 2.** Aerosol optical depth (AOD) (unitless) for (a, b) Intermediate, (c, d) Clean, and (e,f) Extra, shown at 01 UTC 21 Sep 2022 (a,c,e) and 03 UTC 23 Sep 2022 (b,d,f).

Verification against in situ measurements was performed using HALO lidar data from CPEX-CV Research Flights 09 and 10. HALO extinction coefficients at 532 nm were compared with WRF-Chem extinction coefficients at 550 nm, wavelengths 160 close enough for direct comparison. According to the Angstrom Power Law, the differences of these wavelengths are on the order of 3 percent. To remove ice crystal contamination, data points with depolarization ratios greater than 0.3 were masked (Ansmann et al., 2009). Model output was interpolated along the HALO flight paths for direct comparison (Figure 3).

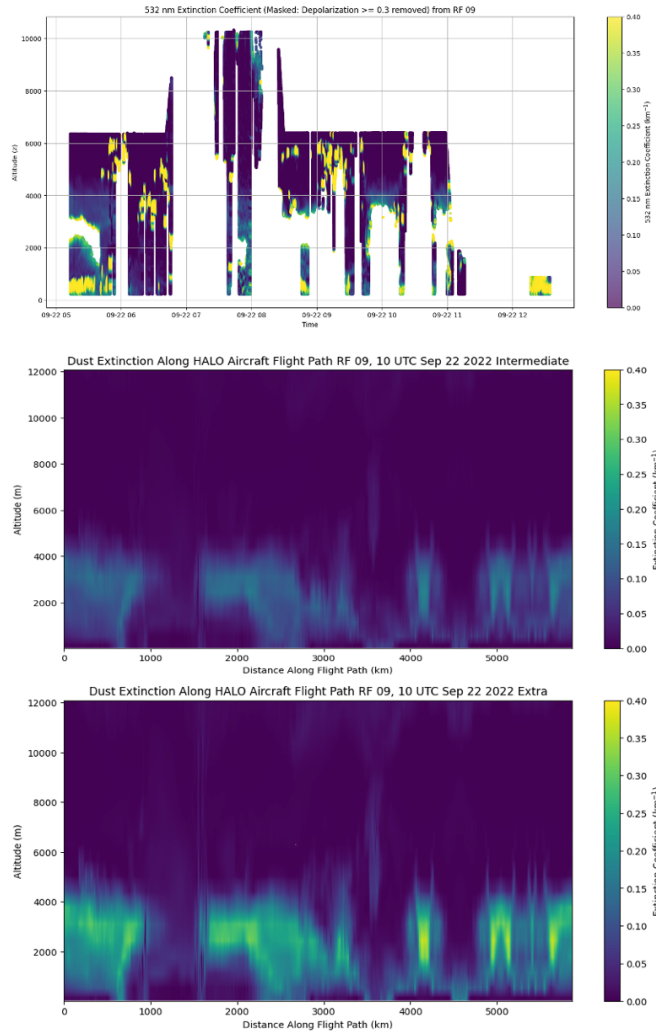


Figure 3. A comparison of extinction coefficients (unit: km^{-1}) at 10 UTC 22 Sep 2022. The top subplot is for RF 09 during
165 CPEX-CV, the middle plot is for Intermediate, and the lowest plot is for Extra.

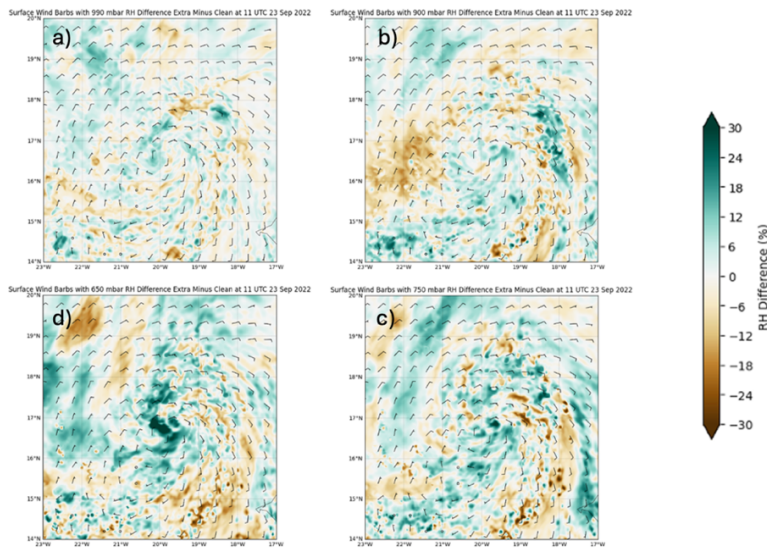
For RF 09, Extra reproduced the vertical extent and spatial placement of the dust plume, with extinction coefficients of 0.2–0.3 km^{-1} below 4 km altitude. Intermediate matched plume location but underestimated magnitudes, producing values around 0.1–0.2 km^{-1} —about half of those observed—likely due to lower CAMS-initialized values. RF 10 provided less
170 coverage but confirmed that Extra was closest to observations once possible ice contamination was accounted for. Across both flights, Intermediate consistently underrepresented dust, validating its role as a lower-bound dust scenario.

3.2 Moisture field

The influence of dust on environmental moisture was assessed by comparing Extra and Clean. Relative humidity (RH)



175 differences (Figure 4) showed that dust increased mid-level moisture, particularly at 650 and 750 hPa, with smaller positive differences near the surface (900 hPa). These results align with Pan et al. (2008), which found that dust acts as cloud condensation nuclei and ice nuclei, promoting cloud formation with smaller droplets that extend the atmospheric residence time of water vapor.



180 **Figure 4.** Relative humidity difference between Clean and Extra at the (a) 990, (b) 900, (c) 750, and (d) 750 mbar levels at 1100 UTC 23 Sep 2022. Blue shading means that Extra was more humid, while tan shading means that Clean was more humid.

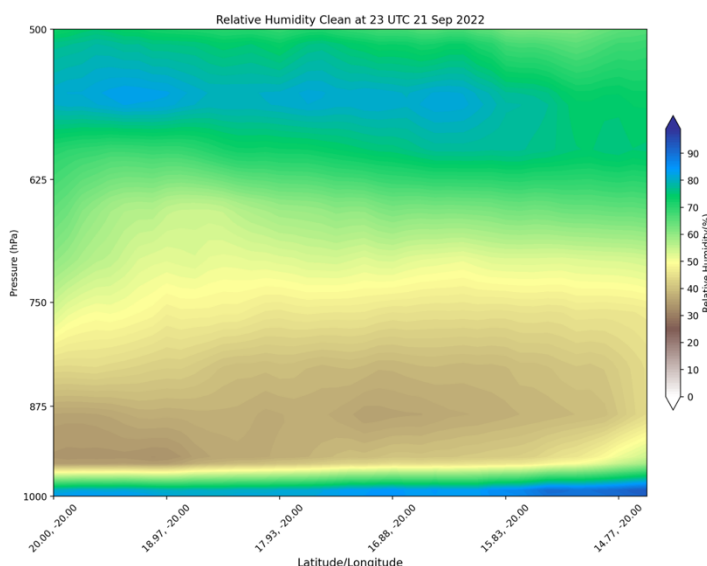


Figure 5. Cross-section of the initial relative humidity (shaded; unit: %) for Clean at 23 UTC 21 Sep 2022 over the area



where Hermine would move in later timesteps. Tan shading indicates dry air, while green and blue shading indicate moist air. The figure is also representative of Intermediate and Extra.

185

Areas of increased RH overlapped with regions of high dust concentration, underscoring the dust–moisture link, driven by radiation changes. All simulations began with identical humidity fields, ensuring that the differences were dust-driven. Figure 5 shows that the initial environment in all runs was dominated by the dry Saharan Air Layer, with very low RH aloft above the marine layer. Even in Clean, the storm developed in an arid environment, making the dust-related mid-level 190 moistening more apparent.

190

3.3 Radiative and thermodynamic effects

Model outputs showed clear differences in the radiative balances. The top-of-atmosphere (TOA) outgoing longwave 195 radiation (OLR) difference between Extra and Clean (Figure 6) showed higher OLR in Extra’s inner core, consistent with dust absorption of shortwave radiation and re-emission in the longwave spectrum. While the absence of clear-sky radiation diagnostics in WRF-Chem prevents fully separating cloud and dust effects, the pattern is consistent with established aerosol–radiation theory.

These radiative impacts translated into thermodynamic changes. Extra was warmer at 600 hPa and cooler at 950 hPa 200 compared to Clean (Figure 7), reducing lapse rates and increasing stability—conditions that suppress tropical cyclone intensification. Latent heat flux differences (Figure 8) showed that Clean had greater surface latent heat fluxes, reflecting stronger surface–atmosphere energy exchange and more vigorous convection. The stability enhancement in Extra likely contributed to reduced convection and latent heat release, further limiting storm growth.

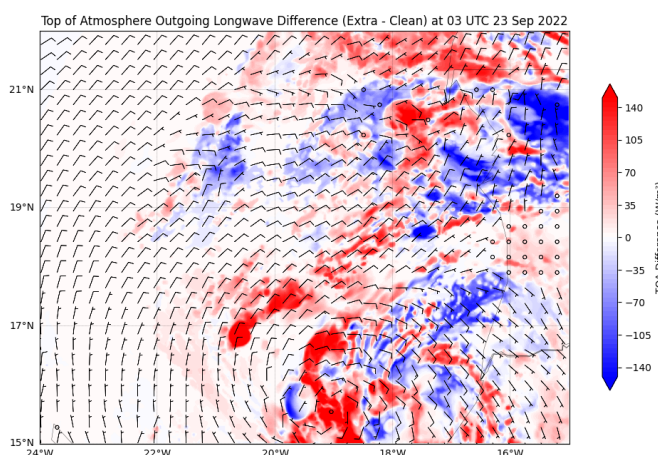


Figure 6. Top of atmosphere outgoing longwave radiation difference (shaded; unit: Wm^{-2}) between Extra and Clean at 03 205 UTC 23 Sep 2022.

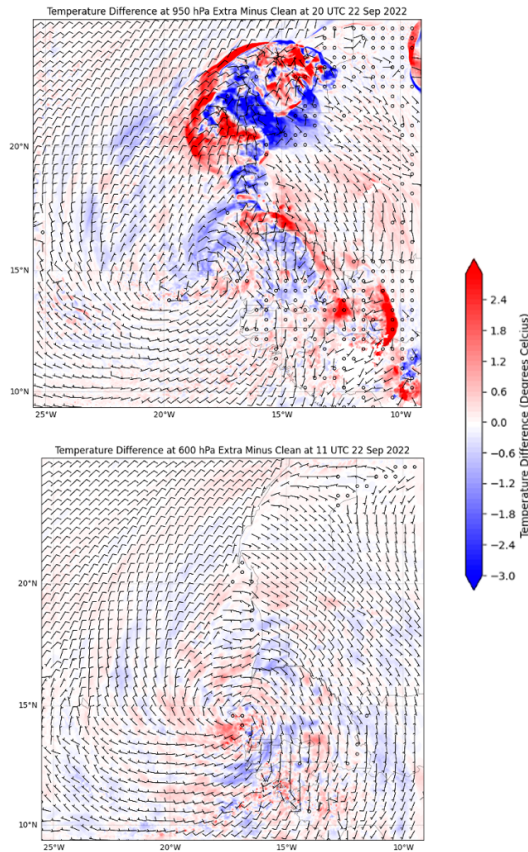


Figure 7. Temperature differences (shaded; unit: °C) between Extra and Clean at the 950 (top) and 600 hPa (bottom) pressure levels with surface wind barbs at 11 UTC 22 Sep 2022. Red values mean that Extra was warmer, while blue values mean that Clean was warmer.

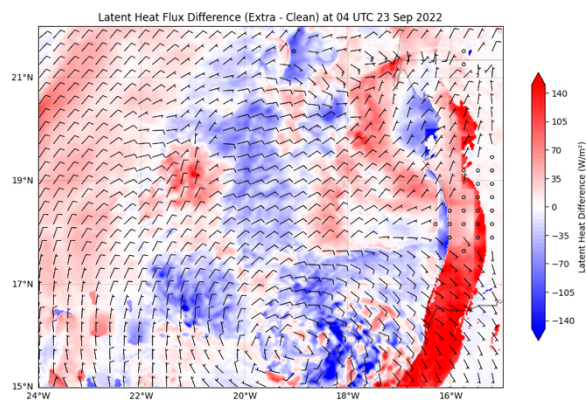


Figure 8. Latent heat flux differences (shaded; unit: W m^{-2}) between Extra and Clean at the surface, with surface wind

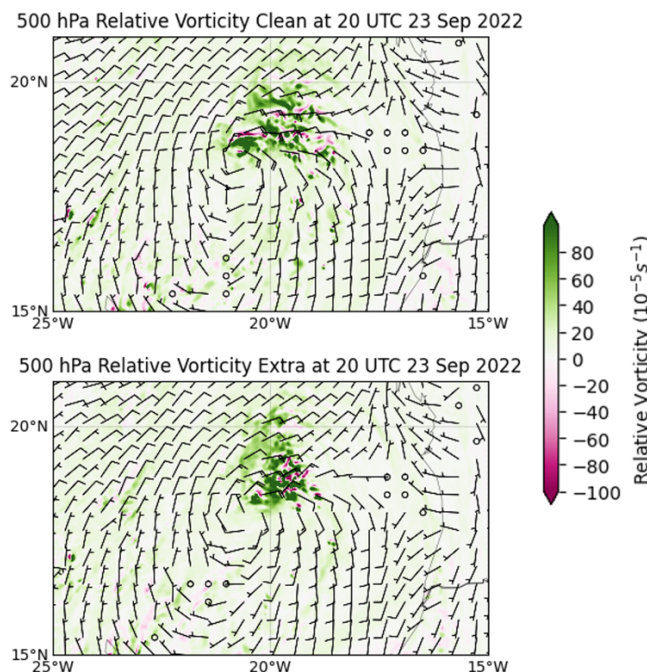


barbs, at 04 UTC on 23 September 2022. To enable a direct comparison, the storms were shifted slightly to align with each other. This shift produced an artifact—an area of high latent heat flux difference—along the West African coast.

215 **3.4 Vertical Motion**

Dust's stabilizing effects were also evident in the storm's kinematic structure. Relative vorticity fields (Figure 9) showed that in Extra, maxima were concentrated in the northeastern quadrant, with minimal inner-core coverage—indicating a more 220 disorganized system. Clean had stronger, more evenly distributed vorticity that extended into the storm center, suggesting healthier organization.

Simulated reflectivity fields (Figure 10) reinforced this finding: while all runs showed a dry southern sector and strongest reflectivity in the northeastern quadrant, Clean's inner-core reflectivity exceeded Extra's by up to 10 dBZ. Vertical velocity plots (Figure 11) revealed that Clean had the most coherent ring of rising motion around the center, stronger sinking motion 225 in the developing eye, and more complete banding structures. Extra's updrafts were weaker and primarily confined to the northern storm sector. In all runs, the western semicircle was weaker than the eastern semicircle, likely due to northward storm motion enhancing convergence on the right-hand side via vector addition.



230 **Figure 9.** 500 mbar relative vorticity (shaded; 10^{-5} s^{-1}) for Clean (top panel) and Extra (bottom panel) at 20 UTC 23 Sep 2022. Green values indicate positive relative vorticity, while pink values indicate negative relative vorticity.

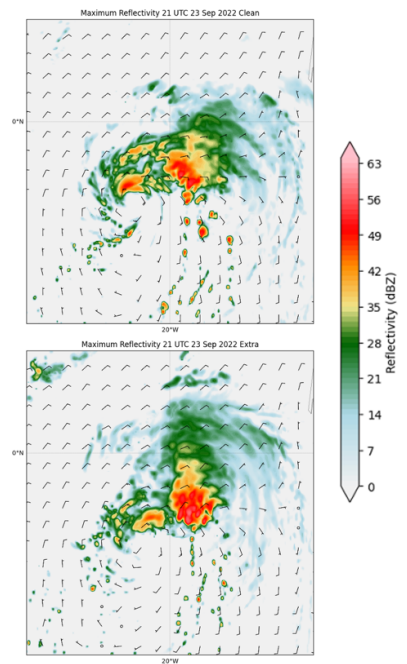


Figure 10. Simulated radar reflectivity (shaded; dBZ) from Clean (top panel) and Extra (bottom Panel) at 21 UTC 23 Sep 235 2022.

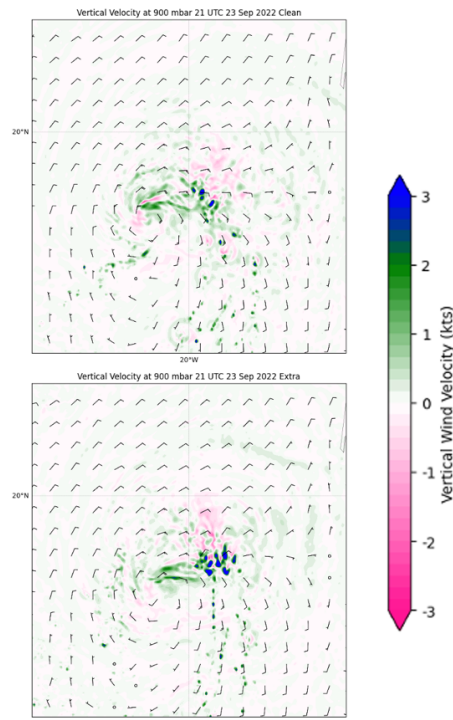




Figure 11. Vertical velocity (shaded; unit: kts) at 900 mb at 21 UTC 23 Sep 2022 from Clean (top panel) and Extra (bottom panel). Greens are upward motion, while pinks are downward motion.

240 3.5 Impacts on Wind and Pressure

Minimum central sea level pressure (MSLP) was used to assess storm intensity. Initially, all runs followed similar evolution due to identical meteorological initializations and model spin-up (Figure 12). Divergence began around 12 UTC 22 September 2022, when Clean deepened more rapidly than the dust-present runs. By the end of the simulation, Clean's MSLP 245 was ~4 hPa lower than Intermediate, with Extra slightly stronger than Intermediate but still weaker than Clean.

Spatial pressure differences between Intermediate and Clean (Figure 13) showed higher central pressures in Intermediate, consistent with weaker intensity. This pattern persisted through the latter half of the simulation period. Wind structure 250 analysis (Figure 14) revealed that Clean had a compact, circular center with a developing eyewall and peak winds near the core, characteristic of organized tropical storms. Extra's center was elongated, with peak winds displaced from the core, indicating a broader and less organized structure. These results support the hypothesis that dust enhances convection in the storm's periphery at the expense of inner- core organization, weakening overall storm structure.

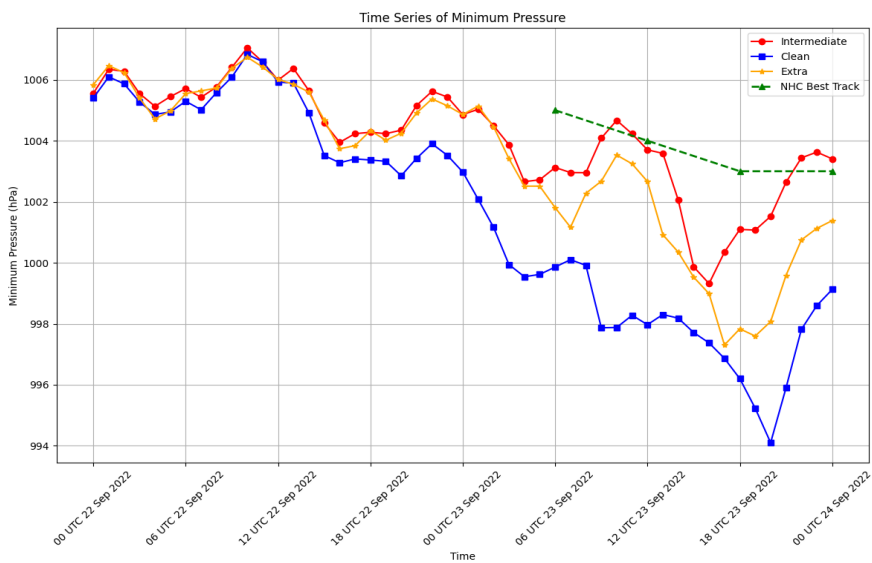


Figure 12. Time series of the storm's central minimum sea level pressure for Intermediate, Clean, and Extra, compared with the NHC best-track data. The red line represents Intermediate, the blue line Clean, and the orange line Extra.

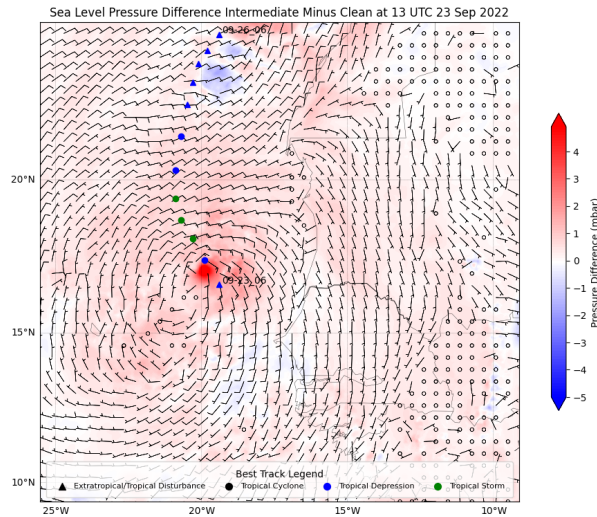


Figure 13. Sea level pressure differences (shaded; unit: mb), calculated by subtracting Clean values from Intermediate values at 13 UTC, 23 September 2022. The dots represent NHC data for comparison. The wind field is the surface wind field.

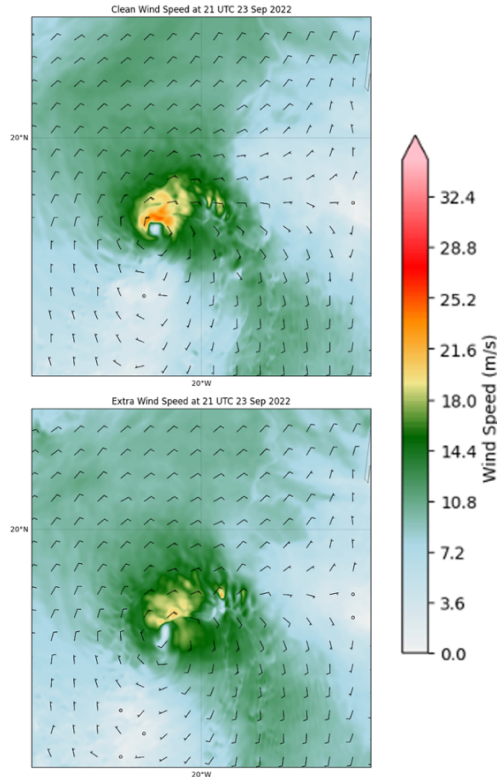


Figure 14. Surface wind speed (shaded; unit: m s^{-1}) and direction for Clean (top panel) and Extra (bottom panel) at 21 UTC on 23 September 2022.



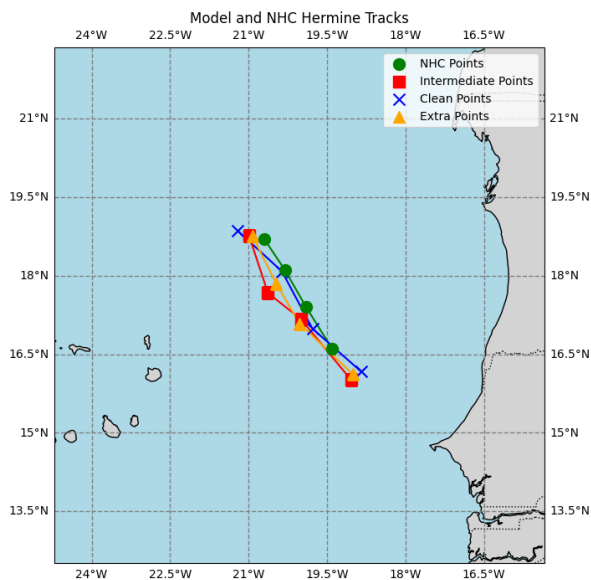
265

3.6 Track Differences

Track comparisons ensured that all storms experienced similar environmental conditions. The positions of the lowest-pressure centers at four-time steps—06, 12, and 18 UTC 23 September, and 00 UTC 24 September—are shown in Figure 15.

270 The tracks remained geographically close throughout, minimizing environmental variability.

Track errors relative to the NHC best track (Table 1) were within typical model error ranges. Extra had the smallest average error, reinforcing its classification as the most observation-consistent simulation in terms of both dust representation and storm track.



275 **Figure 15.** Comparison of the simulated storm tracks with NHC best-track data for the period from 06 UTC on 23 September to 00 UTC on 24 September. The blue line represents the NHC best-track data, the red line Intermediate, the green line Clean, and the yellow line Extra.

280 **Table 1.** Spatial differences between the simulated tracks and the NHC best-track data. Values represent the distance between the simulated storm locations—determined by the minimum sea level pressure—and the center of Hermine, as designated in the NHC best-track data at the corresponding times.



	06 UTC 23 Sept 2022	12 UTC 23 Sept 2022	18 UTC 23 Sept 2022	00 UTC 24 Sept 2022	Average
Intermediate	75 km	28 km	59 km	31 km	48 km
Clean	76 km	48 km	6 km	56 km	47 km
Extra	67 km	37 km	33 km	25 km	41 km

285

4. Discussion and Concluding Remarks

Dust interactions with developing tropical cyclones remain one of the major open questions in tropical meteorology. This study sought to contribute to that understanding through a set of WRF-Chem simulations of Tropical Storm Hermine (2022),
290 supported by in situ observations from the NASA CPEX-CV field campaign. Three primary simulations were examined:

Clean (no dust), Intermediate (moderate dust based on unmodified CAMS initial conditions), and Extra (high dust case, initialized with doubled MOZBC mapping coefficients to match CPEX-CV observations). Research Flights 09 and 10 provided key dust measurements, revealing that CAMS underestimated dust concentrations by roughly 50% in this case—highlighting the importance of direct observations for accurate model initialization.

295 The results consistently showed that dust negatively influenced Hermine's development. The non-dust run, Clean, produced the most intense and best-organized storm, with minimum central pressures more than 4 hPa lower than in either dust-present run. Since initial meteorological conditions were identical across experiments, these differences can be attributed solely to the initial dust loadings. Both Intermediate and Extra yielded weaker systems, with structural characteristics that contrasted sharply with Clean.

300 Detailed diagnostics indicated that these intensity differences were tied to fundamental structural changes in the storm. In Clean, the strongest convection and highest radar reflectivities were concentrated in the inner core, supporting a compact and organized vortex. In contrast, Intermediate and Extra exhibited peak reflectivities in the northeastern quadrant, away from the center, indicative of a disorganized system. Mid-level relative humidity was higher in the dust cases, likely due to dust's role as effective cloud condensation and ice nuclei. This enhancement of mid-level moisture supports the hypothesis (Khain
305 et al., 2009; Zhang et al., 2007) that dust promotes convection on the storm's periphery, diverting energy away from the inner core and limiting intensification.

The chain of impacts observed here aligns with established aerosol–cyclone interaction theory. Dust-induced changes in moisture fields, particularly in the mid- to upper troposphere, altered the storm's radiative budget. In Extra, dust and associated cloud interactions increased top-of-atmosphere outgoing longwave radiation and produced a more stable
310 atmosphere through mid-level warming and near-surface cooling. This enhanced static stability suppressed inner-core



updrafts, reduced vorticity in the center, and shifted convective activity outward. As a result, vertical velocity patterns and reflectivity fields showed more fragmented, asymmetric structures in the dust-present runs.

While the pressure and wind differences were substantial, track impacts were minimal. All runs maintained similar paths, but Extra—initialized with observed dust conditions—had the smallest track errors relative to the NHC best track. This likely
315 reflects the improved realism of its initial conditions rather than a direct dynamical effect of dust on track. Nevertheless, the presence of dust consistently corresponded with less rising motion in the inner core, weaker convergence near the center, and an absence of the early eyewall features seen in Clean.

The role of physics choices in WRF-Chem was also pivotal. As shown in Section 3, when radiative and cloud physics effects were excluded, dust had little influence on storm evolution. This underscores that the aerosol impacts seen here operate
320 primarily through radiative and microphysical pathways, consistent with Khain et al. (2009) and Pan et al. (2018). The enhanced mid-level humidity and reduced organization in the dust cases match the idealized modeling results of Zhang et al. (2007).

It is important to note that these findings are based on a single case study of a relatively weak tropical storm in the eastern
325 Atlantic. Dust–cyclone interactions may differ by region, storm maturity, and environmental context. For example, dust impacts in the Gulf of Mexico may contrast with those over the eastern Atlantic, and major hurricanes may respond differently than weaker storms. Likewise, precursor disturbances might react differently to dust than named storms. These potential variations mean that the conclusions here should not be generalized without caution.

Future research should expand the analysis to multiple storms across diverse basins, incorporating additional observational
330 datasets to validate and refine model results. Key questions include the role of dust introduction timing, the vertical distribution of aerosols, and the mechanisms of dust removal from the atmosphere. The potential microphysical impacts of dust, particularly its role as cloud condensation and ice nuclei, were not explicitly represented in the present simulations. Future studies should incorporate dust–microphysics interactions to better quantify how nucleation processes influence storm structure, precipitation distribution, and intensity. Furthermore, the demonstrated underestimation of dust by CAMS in this
335 case points to the need for improved aerosol data assimilation and greater integration of high-quality observational data into chemistry–weather models. Addressing these issues will be essential for producing more reliable forecasts of dust–cyclone interactions and their implications for storm intensity and structure.

In summary, this study demonstrates that Saharan dust can significantly weaken a developing tropical storm by altering its
340 thermodynamic and microphysical environment. In Hermine’s case, dust increased mid-level humidity, enhanced atmospheric stability, and shifted convection away from the inner core, resulting in a less organized vortex and higher central pressures. These impacts were driven primarily through radiative and cloud microphysics pathways and were most pronounced when realistic, observation-based dust loadings were applied. While track changes were minimal, storm structure and intensity differences were substantial, underscoring the importance of accurate aerosol initialization in numerical models. Broader application of these methods across storms and regions will be essential for determining how general these dust–cyclone interaction mechanisms are.



345

Code, data, or code and data availability

All data used in this study are publicly available online. Data from the Convective Processes Experiment – Cabo Verde (CPEX-CV) field campaign were obtained from NASA's Earth Science Project Office website (<https://espo.nasa.gov/cpex-cv>). Definitions related to tropical systems were obtained from the U.S. National Weather Service Tropical Definitions webpage (https://www.weather.gov/mob/tropical_definitions). Atmospheric reanalysis data were obtained from the ECMWF Reanalysis v5 (ERA5) dataset, available at <https://www.ecmwf.int/en/forecasts/dataset/ecmwf-reanalysis-v5>, and from the CAMS Global Reanalysis EAC4, accessed via the Copernicus Atmosphere Data Store (<https://ads.atmosphere.copernicus.eu/datasets/cams-global-reanalysis-eac4>). Tropical cyclone best-track data for the 2021 Atlantic hurricane season were obtained from the National Hurricane Center archive, available at <https://www.nhc.noaa.gov/data/tcr/index.php?season=2021&basin=atl> (National Hurricane Center and Central Pacific Hurricane Center, 2022).

Supplement link

N/A.

360

Team list

N/A.

Author contributions

365 AG collected the data, performed the experiments, analyzed the experiment results, and drafted the paper. ZP developed the overall research goals and aims, acquired the financial support for the project leading to this publication, and revised the manuscript critically. AGH commented on and revised the manuscript.

Competing interests

370 The authors declare that they have no conflict of interest.

Disclaimer

Copernicus Publications remains neutral with regard to jurisdictional claims made in the text, published maps, institutional affiliations, or any other geographical representation in this paper. While Copernicus Publications makes every effort to 375 include appropriate place names, the final responsibility lies with the authors. Views expressed in the text are those of the authors and do not necessarily reflect the views of the publisher.



Acknowledgements

380 This manuscript is based on the M.S. thesis of the first author (AG). Dr. Greg McFarquhar, who served on the supervisory committee, contributed to this thesis project through useful discussions. Computational support was provided by the University of Utah's Center for High Performance Computing.

Financial support

385 This work was supported by NASA Award #80NSSC23K1289.

Review statement

The review statement will be added by Copernicus Publications.

390 **References**

Ansmann, A., Tesche, M., Seifert, P., Althausen, D., Engelmann, R., Fruntke, J., Wandinger, U., Mattis, I., and Müller, D.: Evolution of the ice phase in tropical altocumulus: SAMUM lidar observations over Cape Verde, *J. Geophys. Res.*, 114, D17208, <https://doi.org/10.1029/2008JD011659>, 2009.

Bercos-Hickey, E., Nathan, T. R., and Chen, S.-H.: Saharan dust and the African easterly jet–African easterly wave system: 395 Structure, location and energetics, *Q. J. R. Meteorol. Soc.*, 143, 2797–2808, <https://doi.org/10.1002/qj.3128>, 2017.

Bhatia, K. T., Vecchi, G. A., Knutson, T. R., Murakami, H., Kossin, J. P., and Dixon, K. W.: Thermodynamic environments around tropical cyclones have become more favorable for intensification, *Nat. Commun.*, 13, 730, <https://doi.org/10.1038/s41467-022-28379-2>, 2022.

Braun, S. A.: Reevaluating the role of the Saharan Air Layer in Atlantic tropical cyclogenesis and evolution, *Mon. Wea. Rev.*, 400 138, 2007–2037, <https://doi.org/10.1175/2009MWR3135.1>, 2010.

Chen, S.-H., and Sun, W.-Y.: A one-dimensional time-dependent cloud model, *J. Meteor. Soc. Japan*, 80, 99–118, <https://doi.org/10.2151/jmsj.80.99>, 2002.

Chicea, D., and Olaru, S.: Profiling particles of Sahara dust settled on the ground by a simplified dynamic light scattering procedure and sedimentation, *Int. J. Environ. Res. Public Health*, 20, 4860, <https://doi.org/10.3390/ijerph20064860>, 2023.

405 Collins, W. D., Rasch, P. J., Boville, B. A., Hack, J. J., McCaa, J. R., Williamson, D. L., Kiehl, J. T., Briegleb, B., Bitz, C., Lin, S.-J., Zhang, M., and Dai, Y.: Description of the NCAR Community Atmosphere Model (CAM 3.0), NCAR Tech. Note, NCAR/TN-464+STR, 1–213, 2004.

DeMaria, M., Knaff, J. A., and Sampson, C. R.: Evaluation of long-term trends in tropical cyclone intensity forecasts, *Meteorol. Atmos. Phys.*, 97, 19–28, <https://doi.org/10.1007/s00703-006-0241-4>, 2007.

410 DeMott, P., et al.: African dust aerosols as atmospheric ice nuclei, *Geophys. Res. Lett.*, 30, 1732, <https://doi.org/10.1029/2003GL017410>, 2003.

ECMWF: ECMWF Reanalysis v5 (ERA5), ECMWF [data set], <https://www.ecmwf.int/en/forecasts/dataset/ecmwf->



[reanalysis-v5](#), accessed 19 March 2024, 2024.

ECMWF: CAMS Global Reanalysis EAC4, Copernicus Atmosphere Monitoring Service [data set],

415 <https://ads.atmosphere.copernicus.eu/datasets/cams-global-reanalysis-eac4>, accessed 10 April 2025, 2025.

Emanuel, K.: Environmental factors affecting tropical cyclone power dissipation, *J. Climate*, 20, 5497–5509,

<https://doi.org/10.1175/2007JCLI1571.1>, 2007.

Grell, G. A.: Prognostic evaluation of assumptions used by cumulus parameterizations, *Mon. Wea. Rev.*, 121, 764–787,

[https://doi.org/10.1175/1520-0493\(1993\)121<0764:PEOAUB>2.0.CO;2](https://doi.org/10.1175/1520-0493(1993)121<0764:PEOAUB>2.0.CO;2), 1993.

420 Harrison, A. D., et al.: The ice-nucleating activity of African mineral dust in the Caribbean boundary layer, *Atmos. Chem. Phys.*, 22, 9663–9680, <https://doi.org/10.5194/acp-22-9663-2022>, 2022.

Inness, A., Engelen, R., and Flemming, J.: The new CAMS global reanalysis of atmospheric composition, ECMWF Newsletter, 158, <https://www.ecmwf.int/en/newsletter/158/meteorology/new-cams-global-reanalysis-atmospheric-composition>, accessed 15 April 2024, 2019.

425 Kazil, J.: Introduction to aerosol modeling with WRF/Chem, Cooperative Institute for Research in Environmental Sciences, University of Colorado and NOAA, Online presentation,

https://www.mce2.org/Kazil_2009_07_22_Tutorial%20%28Rainer%29.pdf, accessed 10 April 2025, 2009.

Khain, A., Lynn, B., and Dudhia, J.: Aerosol effects on intensity of landfalling hurricanes as seen from simulations with the WRF model with spectral bin microphysics, *J. Atmos. Sci.*, 67, 365–384, <https://doi.org/10.1175/2009JAS3210.1>, 2010.

430 Knippertz, P., and Todd, M. C.: Mineral dust aerosols over the Sahara: Meteorological controls on emission and transport and implications for modeling, *Rev. Geophys.*, 50, RG1007, <https://doi.org/10.1029/2011RG000362>, 2012.

Mlawer, E. J., Taubman, S. J., Brown, P. D., Iacono, M. J., and Clough, S. A.: Radiative transfer for inhomogeneous atmospheres: RRTM, a validated correlated-k model for the longwave, *J. Geophys. Res.*, 102, 16663–16682, <https://doi.org/10.1029/97JD00237>, 1997.

435 NASA: Convective Processes Experiment – Cabo Verde (CPEX-CV), NASA [project], <https://espo.nasa.gov/cpex-cv/>, accessed 19 March 2024, 2024.

Nowotnick, E. P., et al.: Dust, convection, winds, and waves: the 2022 NASA CPEX-CV Campaign, *Bull. Amer. Meteor. Soc.*, 105, E2097–E2125, <https://doi.org/10.1175/BAMS-D-23-0201.1>, 2024.

Pan, B., et al.: Impacts of Saharan dust on Atlantic regional climate and implications for tropical cyclones, *J. Climate*, 31, 440 7621–7644, <https://doi.org/10.1175/JCLI-D-16-0776.1>, 2018.

Reale, O., Lau, W. K., Kim, K.-M., and Brin, E.: Atlantic tropical cyclogenetic processes during SOP-3 NAMMA in the GEOS-5 global data assimilation and forecast system, *J. Atmos. Sci.*, 66, 3563–3578, <https://doi.org/10.1175/2009JAS3123.1>, 2009.

445 Reinhart, B.: Tropical Cyclone Report: Tropical Storm Hermine, National Hurricane Center, https://www.nhc.noaa.gov/data/tcr/AL102022_Hermine.pdf, accessed 28 March 2024, 2023.

Skamarock, W. C., et al.: A description of the Advanced Research WRF version 4.1, NCAR Tech. Note, NCAR/TN-



556+STR, 162 pp., <https://doi.org/10.5065/1dfh-6p97>, 2019.

Skamarock, W. C., Ong, H., and Klemp, J. B.: A fully compressible nonhydrostatic deep-atmosphere equations solver for MPAS, *Mon. Wea. Rev.*, 149, 571–583, <https://doi.org/10.1175/MWR-D-20-0286.1>, 2021.

450 Skamarock, W. C., Klemp, J. B., Duda, M. G., Fowler, L. D., Park, S., and Ringler, T. D.: A multiscale nonhydrostatic atmospheric model using centroidal Voronoi tessellations and C-grid staggering, *Mon. Wea. Rev.*, 140, 3090–3105, <https://doi.org/10.1175/MWR-D-11-00215.1>, 2012.

Takahashi, C., Watanabe, S., Kawatani, M., Abe, M., and Takata, M.: Sulfate aerosols and reduced tropical cyclone frequency in the western North Pacific, *Geophys. Res. Lett.*, 44, 7519–7527, <https://doi.org/10.1002/2017GL073239>, 2017.

455 Zauli Sajani, S., Bonasoni, P., Cristofanelli, P., Marinoni, A., and Lauriola, P.: Only coarse particles from the Sahara?, *Epidemiology*, 23, 642–643, <https://doi.org/10.1097/EDE.0b013e318258c23f>, 2012.

Zhang, H., McFarquhar, G., Saleeby, S., and Cotton, W.: Impacts of Saharan dust as CCN on the evolution of an idealized tropical cyclone, *Geophys. Res. Lett.*, 34, L14812, <https://doi.org/10.1029/2007GL029876>, 2007.

460